Assumption-free measurement of the quantum state of light: Exploring the sidebands of intense fields

F. A. S. Barbosa [●],[1] A. S. Coelho,[2,3] K. N. Cassemiro,[4] M. Martinelli [●],[5] P. Nussenzveig,[5] and A. S. Villar[4,*]

[1]*Instituto de Física Gleb Wataghin, Universidade Estadual de Campinas, 13083-859 Campinas, SP, Brazil*
[2]*Departamento de Engenharia Mecânica, Universidade Federal do Piauí, 64049-550 Teresina, PI, Brazil*
[3]*Departamento de Engenharia, Centro Universitário UNINOVAFAPI, 64073-505 Teresina, PI, Brazil*
[4]*American Physical Society, 1 Research Road, Ridge, New York 11961, USA*
[5]*Instituto de Física da Universidade de São Paulo, P.O.Box 66318, 05315-970 São Paulo, Brazil*

The quantum noise in photocurrent fluctuations usually gives incomplete information about the quantum state of spectral sideband modes of bright light beams involved in the detection. Each frequency component of the noise spectrum corresponds to two sideband modes symmetrically located around the bright optical field. In the case of the usual homodyne detection, it limits the ability to recover discriminated information of each mode involved. We theoretically show that complete reconstruction of the two-mode quantum state can be obtained by using phase-locked (coherent) resonator detection, even for non-Gaussian states. We experimentally demonstrate the technique by measuring a two-mode displaced coherent state.

I. INTRODUCTION

Measurement of the noise of light is the main experimental tool to provide information of the quantum state of spectral modes in the continuous variables (CV) picture, in which observables involving quadratures of the electromagnetic field are used. However, the usual procedure to access it provides neither a pure nor a complete quantum measurement of the two-mode spectral quantum state [1,2], due to lack of phase coherence in the measurement process. Measurement mixedness currently restricts the faithful reconstruction of spectral quantum states to those presenting spectrally uniform energy distribution and Gaussian statistics, requiring the use of *a priori* knowledge to achieve complete reconstruction [1]. For this particular class of quantum states, it is possible to realize a pure quantum measurement of "effective" single-mode quadrature operators [2].

The two-mode spectral state measurement has been successfully utilized from the first experimental demonstrations of quantum noise squeezing to the more recent observation of tripartite entanglement of spectral modes [3–9]. A major breakthrough was achieved in a recent experiment [10], where distinct second-order momenta of the quadratures of the field where measured by intensity measurement combined with parametric amplification. The method allowed the direct observation of squeezing spanning a 55-THz bandwidth. This combination of parametric amplifiers for nonclassical state generation and further reading of the state was also explored in other measurement situations [11], either in interferometric measurements [12], teleportation protocols [13], or computation proposals [14].

Nevertheless, the experimental capability to unambiguously establish non-Gaussian features of the spectral quantum state is fundamentally important to move forward and consider more general quantum states of sideband modes [15–19]. The characterization and control of any unknown quantum state of spectral field modes requires the availability of a complete set of quantum measurements. We have shown in a recent paper that the measurement technique of resonator detection (RD) is able to access alternative aspects of each individual spectral mode even in the realistic nonideal scenario of phase mixed quantum noise by achieving an effective spatial separation of the sidebands [1,20]; moreover, RD is "complete" in the sense that it furnishes all the available information in this restricted scenario. In this case, the measured quantum noise reveals additional information about the energy distribution in the two spectral sideband modes, a feature always missed by the widely employed measurement technique of spectral homodyne detection (HD). Even though the Gaussian character of the photocurrent statistics can be used to partially "undo" the incoherent effects introduced by phase mixing [19], *a priori* knowledge about the Gaussian character of the quantum state is still assumed even in this favorable case.

In this paper, we introduce phase coherence on the RD technique, resulting in a pure and complete measurement operator for the two spectral sideband modes, removing the necessity of *a priori* assumptions about the quantum state. Our method fixes the incoherence gap in the downmixing chain by employing the electronic local oscillator (eLO), as well as the optical LO, to produce the quantum state and thus ensure phase coherence between both signals [21]. In this experimental scenario, we employ RD to investigate a two-mode spectral quantum state produced by "phase modulation" of a laser

---

*villar@if.usp.br

beam [22]. Finally, we investigate in theory the circumstances under which resonator detection yields a pure and complete quantum measurement.

These results generalize previous investigations where we have shown that RD achieves complete reconstruction of Gaussian quantum states if they are compatible with the usual incoherent detection scheme, a scenario limiting the information of the two mode quantum state to only four second-order quadrature moments [1,2]. We now show RD to provide complete access to the four-dimensional phase space of two spectral modes, thus being able to reconstruct (assumption-free) any Wigner function by CV quantum state tomography [23,24]. For Gaussian states, this means complete access to all the ten moments of the covariance matrix. Realistic limitations of the technique are investigated by explicitly considering the occurrence of spatial modal mismatch in the measurement setup. This measurement procedure should allow one to reconstruct arbitrary four-dimensional Wigner functions, in particular bringing the capability to unambiguously identify non-Gaussian features in the two-mode spectral quantum noise measurement [17,19].

We organize this paper as follows. In Sec. II, the basic theory is developed to show what is expected from a complete two-mode measurement and how RD is able to achieve those requirements. We also investigate the effect of spatial mode mismatch in the measurement operator of RD. In Sec. III, we realize the experimental implementation of coherent RD applied to the simplest two-mode quantum state possessing phase information: a coherent state produced by classical phase modulation. By keeping track of the spectral phase used in the electronic process of acquiring the Fourier components of the quantum noise, we are able to show phase sensitivity beyond what is currently attained in usual experiments. We offer our concluding remarks in Sec. IV

II. PHASE COHERENT RESONATOR DETECTION

The measurement technique of resonator detection is based on the dispersive property of an optical resonance [25–27]. The quantum field of interest is first combined with the optical reference field (LO) and then reflected off an optical resonator; the total field is then detected and the beatnote signal analyzed. Due to the frequency-dependent phase shift and (crucially) modal attenuation, properties of individual spectral modes become accessible in the quantum noise. In particular, selective modal attenuation provides experimental access to the energy imbalance between spectral modes even in the phase mixing regime, a feature not recoverable with spectral HD [1].

A. Spectral photocurrent

In the general context of spectral quantum noise measurements, the longitudinal modes of interest reside in the vicinity of the LO (with optical frequency ω_0), separated from it by a beatnote frequency $\Omega \ll \omega_0$ (both defined as positive) that will be selected at the detection by the electronic reference. The upper sideband mode corresponds to the optical frequency $\omega_u = \omega_0 + \Omega$ and the lower sideband mode has the optical frequency $\omega_\ell = \omega_0 - \Omega$. The LO is taken as an

effective coherent state, with amplitude $\alpha = |\alpha| \exp(i\xi)$. The Fourier component $\hat{I}_\Omega$ of the photocurrent quantum noise at beatnote frequency Ω is described by the compact operator

$$\hat{I}_\Omega = \frac{\alpha^*}{|\alpha|} \hat{a}_{\omega_0 - \Omega} + \frac{\alpha}{|\alpha|} \hat{a}^\dagger_{\omega_0 + \Omega}, \qquad (1)$$

from which the two Hermitian observables corresponding to the cosine $\hat{I}_{\cos} = \frac{1}{2}(\hat{I}_\Omega + \hat{I}_{-\Omega})$ and sine $\hat{I}_{\sin} = \frac{-i}{2}(\hat{I}_\Omega - \hat{I}_{-\Omega})$ photocurrent components can be determined. For each mode, the photon annihilation $\hat{a}_\omega$ and creation $\hat{a}^\dagger_\omega$ operators satisfy $[\hat{a}_\omega, \hat{a}^\dagger_{\omega'}] = \delta(\omega - \omega')$, where ω is the optical frequency labeling each mode. It is clear from Eq. (1) that both spectral sideband modes contribute to the quantum noise.

The annihilation and creation operators in Eq. (1) can be eliminated in favor of the amplitude $\hat{p}_\omega$ and phase $\hat{q}_\omega$ field quadratures, which obey the commutation relation $[\hat{p}_\omega, \hat{q}_{\omega'}] = 2i\delta(\omega - \omega')$, and read as $\hat{p}_\omega = \hat{a}_\omega + \hat{a}^\dagger_\omega$ and $\hat{q}_\omega = -i(\hat{a}_\omega - \hat{a}^\dagger_\omega)$. This procedure reveals the symmetric ($\mathcal{S}$) and antisymmetric ($\mathcal{A}$) modal combinations of spectral modes as the 'natural' modes of CV detection, represented by the quadrature observables [2]

$$\hat{p}_s = \frac{1}{\sqrt{2}}(\hat{p}_{\omega_u} + \hat{p}_{\omega_\ell}), \qquad \hat{p}_a = \frac{1}{\sqrt{2}}(\hat{p}_{\omega_u} - \hat{p}_{\omega_\ell}),$$

$$\hat{q}_s = \frac{1}{\sqrt{2}}(\hat{q}_{\omega_u} + \hat{q}_{\omega_\ell}), \qquad \hat{q}_a = \frac{1}{\sqrt{2}}(\hat{q}_{\omega_u} - \hat{q}_{\omega_\ell}). \qquad (2)$$

In HD, the cosine photocurrent component measures only $\mathcal{S}$ modal quadratures, whilst the sine component yields access to the $\mathcal{A}$ mode. RD does not reveal a preferred modal basis.

In most experiments, the Fourier amplitude of Eq. (1) is probed only for its total energy, in which case phase information about the cosine and sine components are dismissed as irrelevant. Such approach is valid if one assumes Gaussian quantum states with uniform spectral energy distribution, in which case only second-order quadrature operator moments carry some interest [1,2]. However, for the quantum measurement to be considere pure, phase coherence must exist between the spectral component of the quantum noise and the spectral quantum state: one requires the ability to coherently distinguish between the cosine and sine photocurrent components. We refer to this improved situation as "*phase coherent detection*," which we will explore in the present article.

B. General form of a complete two-mode measurement

The quantum state of a single-mode field can be represented on the phase space of CV quadrature observables [28]. A complete single-mode quantum measurement must be able to determine any field quantum state $\hat{\rho}_\omega$. For instance, in the basis of eigenstates of $\hat{q}_\omega$, that would mean all matrix elements of the form $\langle q_\omega | \hat{\rho}_\omega | q'_\omega \rangle$, where q_ω and q'_ω are eigenvalues of $\hat{q}_\omega$, must be accessible by measurement for the desired range of eigenvalues.

In the case of direct photodetection, only the diagonal matrix elements are available, a problem solved by measuring the same quantum state on many different bases (i.e., eigenstates of any combination of $\hat{q}_\omega$ and $\hat{p}_\omega$) by means of interferometric techniques such as HD. Borrowing measurement tools from standard techniques of quantum optics, quantum state tomography in phase space realizes precisely that [23]. In

fact, the favored point of view of CV quantum optics depicts the quantum state by quasiprobability distributions in phase space such as the Wigner function. For two-mode fields, the Wigner function exists in a four-dimensional phase space. Complete quantum state reconstruction requires the quantum measurement to access the probability distribution associated with any direction in the four-dimensional space.

In the simpler case of a single-mode field (a subspace of the two-mode case), a complete measurement is required to deliver the family of local observables

$$\hat{X}_\omega(\varphi) = \cos\varphi \ \hat{p}_\omega + \sin\varphi \ \hat{q}_\omega. \tag{3}$$

Each measurement operator $\hat{X}_\omega(\varphi)$ represents a direction of observation in the two-mode phase space controlled by the external parameter φ. By measuring the probability distribution of $\hat{X}_\omega(\varphi)$ and varying φ, one is able to reconstruct a quasiprobability distribution in two dimensions. In HD, φ is taken as the phase of the optical local oscillator.

Generalizing this idea, the reconstruction of the quantum state of a two-mode field comprised by optical modes ω and ω' requires additional access to the local observables of the single-mode field ω' given by

$$\hat{X}_{\omega'}(\phi) = \cos\phi \ \hat{p}_{\omega'} + \sin\phi \ \hat{q}_{\omega'}, \tag{4}$$

where the direction of observation in phase space is controlled by a second *independent* phase ϕ of rotation.

As the general case observed in Refs. [2,10], a linear combination on modes is observed in a single detector. Therefore, accessing two-mode coherences also requires the ability to perform a change of *modal* basis, by coherently combining the two modes as in

$$\hat{X}_{\omega,\omega'}(\varphi,\phi,\theta) = \cos\theta \ \hat{X}_\omega(\varphi) + \sin\theta \ \hat{X}_{\omega'}(\phi), \tag{5}$$

where θ controls the relative contribution of modes ω and ω' to the measurement operator. Thus a complete two-mode observable could be of the form

$$\begin{aligned}\hat{X}_{\omega,\omega'}(\varphi,\phi,\theta) = &\cos\theta\cos\varphi \ \hat{p}_\omega + \cos\theta\sin\varphi \ \hat{q}_\omega \\ &+ \sin\theta\cos\phi \ \hat{p}_{\omega'} + \sin\theta\sin\phi \ \hat{q}_{\omega'}.\end{aligned} \tag{6}$$

The probability distribution associated with this observable provides information on the four-dimensional Wigner function of the two modes. A complete measurement on this four dimensional space (involving two conjugate quadratures for each mode of the field) will thus depend on at least three parameters. Parameters φ and ϕ will span the quadratures of each individual mode, while parameter θ will span the contribution of each mode to the final observable.

From this expression, it is clear that any planar 'slice' of the entire phase space could be accessed. For instance, the $\mathcal{S}$ and $\mathcal{A}$ modes would be measured by $\hat{X}_{\omega,\omega'}(\varphi,\varphi,\pi/4)$ and $\hat{X}_{\omega,\omega'}(\varphi,\varphi,-\pi/4)$, respectively, while the observable $\hat{X}_{\omega,\omega'}(\varphi,\varphi+\pi/2,\theta)$ would map two-mode correlations between any quadrature of $\mathcal{S}$ and $\mathcal{A}$. Quantum tomography in phase space could hence be in principle realized [24].

We note that the set of measurements available to spectral HD, even in the ideal case of phase coherent detection, is given by the family of observables $X_{\omega_u,\omega_\ell}(\varphi,\varphi,\theta)$, i.e., limited by the condition $\varphi = \phi$, since only one controllable phase—the LO phase—is available [1,2]. The technique is

thus inherently limited in scope and incapable of accessing the complete two-mode phase space of spectral modes. As presented next, RD does not endure such limitations.

C. Phase coherent RD as a complete quantum measurement

The actual observables associated with the RD quantum measurement are the photocurrent components $\hat{J}_{\cos}$ and $\hat{J}_{\sin}$ defined by the identity $\hat{J}_\Omega = (\hat{J}_{\cos} + i\hat{J}_{\sin})/\sqrt{2}$ measured after the reflection of the fields from a cavity with a high-finesse optical resonance centered at frequency ω_c with bandwidth 2γ. They are dependent on the cavity detuning $\Delta = (\omega - \omega_c)/\gamma$, as defined in Ref. [2] and further discussed in the Appendix A. To be accessed, a well defined phase relation between the optical LO and the electronic local oscillator (eLO) reference used to extract the photocurrent Fourier Ω component is required. In most experiments, incoherence in the spectral analysis leads to the spectrum noise power $S(\Omega) = \langle \hat{J}_\Omega \hat{J}_{-\Omega} \rangle$ as the sole meaningful quantity amenable to measurement [19].

Phase coherent detection brings one additional controllable parameter to the phase space measurement. Any combination of the spectral observables $\hat{J}_{\cos}$ and $\hat{J}_{\sin}$ becomes available by tuning the relative phase Θ between the optical LO and the eLO. Phase coherence implies that the spectral component of Eq. (1) could also be chosen as $\hat{I}_\Omega \rightarrow e^{i\Theta}\hat{I}_\Omega$, where Θ becomes a controllable parameter. The form of the general quantum measurement of phase coherent resonator detection is hence $\hat{J}_\Theta = \cos\Theta \ \hat{J}_{\cos} + \sin\Theta \ \hat{J}_{\sin}$, with $[\hat{J}_{\cos}, \hat{J}_{\sin}] = 0$ (i.e., they are compatible measurements).

We now analyze the RD measurement operator of Eq. (A5) to show that it realizes the general two-mode measurement of Eq. (6), proving in this manner that the technique yields a complete measurement by accessing any direction of observation of the four-dimensional Wigner function in phase space. In doing so, we substitute in Eq. (A5) the field annihilation and creation operators in favor of the quadrature observables. We either choose the spectral ($\hat{p}_{\pm\Omega}$ and $\hat{q}_{\pm\Omega}$) or the $\mathcal{S}/\mathcal{A}$ modal quadrature operators defined in Eq. (2) as convenient. We consider at first the scenario of a narrow linewidth resonator ($\gamma \ll \Omega$) for the sake of clarity.

Starting from the extreme scenario of an ideal lossless resonator ($d = 1$), for which $|R_\Omega(\Delta)| = 1$, the Hermitian observables $\hat{J}_{\cos}$ and $\hat{J}_{\sin}$ establish in this case that $\mathcal{S}$ and $\mathcal{A}$ modes form a privileged modal basis of measurement in all three detuning regions, since Eq. (A5) yields simply

$$\hat{J}_{\cos} \approx \cos\Psi \ \hat{p}_s + \sin\Psi \ \hat{q}_s, \tag{7}$$

$$\hat{J}_{\sin} \approx -\sin\Psi \ \hat{p}_a + \cos\Psi \ \hat{q}_a, \tag{8}$$

where we disregarded global phases that don't contribute to the measurement. Different detuning regions will change the argument of Ψ in these expressions, but not the *form* of the measurement operators.

Equations (7) and (8) indicate that the quantum measurement associated with the lossless resonator finds simple description in the $\mathcal{S}$ and $\mathcal{A}$ modal basis. This fact comes as no surprise, since a lossless resonator can only provide spectral phase shifts and hence makes RD *equivalent* to HD. In fact, although these modes can be individually measured, their

local rotations can not be made independent, as required for a complete two-mode measurement [Eqs. (3) and (4)]: just as in HD, modes $\mathcal{A}$ and $\mathcal{S}$ are both rotated in phase space by one and the same parameter Ψ. The most general measurement operator $\hat{J}_{\Theta}$ coherently combines $\hat{J}_{\cos}$ and $\hat{J}_{\sin}$, as in Eq. (5). For a lossless resonator, it assumes the same form in the three detuning regions,

$$\hat{J}_{\Theta} \approx \cos \Theta (\cos \Psi \, \hat{p}_s + \sin \Psi \, \hat{q}_s) \\ + \sin \Theta (-\sin \Psi \, \hat{p}_a + \cos \Psi \, \hat{q}_a). \quad (9)$$

As it was pointed in Refs. [2,10], $\hat{J}_{\cos}$ and $\hat{J}_{\sin}$ are commuting operators, and can be simultaneously measured by the splitting of the detected signal, once it is properly amplified into a "classical" regime. It is interesting to notice that evaluation of $\hat{J}_{\Theta}$ can give the mean values for each one of the $\mathcal{S}/\mathcal{A}$ modal quadrature operator, but second order momenta cannot be fully evaluated, what is consistent with the demand of Eq. (6) for a complete span of the four dimensional space in order to make a tomographic reconstruction of the state.

Performing a change of modal basis, in terms of spectral sideband quadratures this expression reads as

$$\hat{J}_{\Theta} \approx \frac{1}{\sqrt{2}} \cos(\Theta + \Psi) \, \hat{p}_{\Omega} + \frac{1}{\sqrt{2}} \sin(\Theta + \Psi) \, \hat{q}_{\Omega} \\ + \frac{1}{\sqrt{2}} \cos(\Theta - \Psi) \, \hat{p}_{-\Omega} - \frac{1}{\sqrt{2}} \sin(\Theta - \Psi) \, \hat{q}_{-\Omega}, \quad (10)$$

from which it becomes clear, by comparison with Eq. (6), that resonator detection without modal attenuation can not attain a complete two-mode quantum measurement. The missing sectors of the four-dimensional phase space are in this case the same as in HD, and correspond to the energy asymmetry of spectral sideband modes or, on the $\mathcal{S}$ and $\mathcal{A}$ modal basis, to certain correlations involving the same direction of observation in phase space for both modes [1].

The second extreme working scenario of resonator detection corresponds to the ideal impedance-matched resonator ($d = 0$), for which the mode at exact resonance is completely replaced in reflection by a mode in the vacuum state. The measurement operators $\hat{J}_{\cos}$ and $\hat{J}_{\sin}$ show different features in this limit.

We will now analyze the transformation of these operators in three detuning regions depending on which mode is close to the cavity resonance. For the resonance of the upper sideband, we will call it region 1. For the resonance of the optical carrier it will be named region 2, and finally, for the lower sideband we name it region 3.

In detuning region 2, the resonator acts mainly on the LO field: while attenuation decreases the gain of quantum noise in the downmixing process, it does not affect the general form of the measurement operator and the LO phase shift continues to reproduce the modal transformation provided by HD. Hence the operator of Eq. (9) describes the quantum measurement performed by RD with an impedance-matched resonator close to resonance with the LO. In this detuning region, the technique accesses the single-mode quantum state of $\mathcal{A}$ and $\mathcal{S}$ modal basis and their correlations exactly as HD.

The "hidden" sector of the two-mode quantum state is revealed in detuning regions 1 and 3. In region 1, the resonator

attenuates and phase-shifts the upper sideband mode, reflecting LO and lower sideband with no change. Equation (A7) provides the observables

$$\hat{J}_{\cos} \approx \sqrt{1 - T_{\Omega}} (\cos \Psi_{\Omega} \, \hat{p}_{\Omega} - \sin \Psi_{\Omega} \, \hat{q}_{\Omega}) + \hat{p}_{-\Omega} \\ + \sqrt{T_{\Omega}} \, \hat{u}, \quad (11)$$

$$\hat{J}_{\sin} \approx \sqrt{1 - T_{\Omega}} (\sin \Psi_{\Omega} \, \hat{p}_{\Omega} + \cos \Psi_{\Omega} \, \hat{q}_{\Omega}) - \hat{q}_{-\Omega} \\ + \sqrt{T_{\Omega}} \, \hat{v}, \quad (12)$$

where $\hat{u}$ and $\hat{v}$ represent orthogonal quadratures of a mode in the vacuum state and notation has been simplified to $T_{\Omega} = T(\Delta + \Omega/\gamma)$ and $\Psi_{\Omega} = \Psi(\Delta + \Omega/\gamma)$.

We note that as expected the $\mathcal{S}/\mathcal{A}$ modal basis becomes a convenient measurement basis in case the resonator is far off resonance, since $\Psi(\Delta \ll -\Omega/\gamma) \to 0$. Also of particular interest is the situation at exact resonance with the upper sideband ($\Delta = -\Omega/\gamma$): for such detuning, the two spectral photocurrent components perform a simultaneous measurement of lower sideband conjugate quadratures, since in this special case

$$\hat{J}_{\cos} = \hat{p}_{-\Omega} + \hat{u} \quad \text{and} \quad \hat{J}_{\sin} = -\hat{q}_{-\Omega} + \hat{v}. \quad (13)$$

The added vacuum noise ensures the typical 3-dB noise penalty of simultaneous measurements of noncommuting observables [29]. In fact, phase coherent detection allows any direction of observation in the phase space of lower sideband when the resonator is perfectly tuned to the upper sideband, since in this case the measurement operator reads as

$$\hat{J}_{\Theta} = \cos \Theta \, \hat{p}_{-\Omega} - \sin \Theta \, \hat{q}_{-\Omega} + \hat{u}', \quad (14)$$

where the single-mode vacuum mode operator has been redefined as $\hat{u}'$ by a convenient change of modal basis. This measurement operator has the form of the single-mode observable of Eq. (3) needed as part of a complete two-mode measurement.

In general, the measurement operator in region 1 [Eq. (14)] represents arbitrary changes of modal basis. In fact, the observables of Eqs. (11) and (12) are better visualized as

$$\hat{J}_{\cos} \approx \hat{p}_{-\Omega} + \cos \xi_{\Omega} \hat{X}_{\Omega}(\Psi) + \sin \xi_{\Omega} \hat{u}, \quad (15)$$

$$\hat{J}_{\sin} \approx -\hat{q}_{-\Omega} + \cos \xi_{\Omega} \hat{X}_{\Omega}(\Psi - \pi/2) + \sin \xi_{\Omega} \hat{v}, \quad (16)$$

where $\cos \xi_{\Omega} = \sqrt{1 - T_{\Omega}}$ and $\sin \xi_{\Omega} = \sqrt{T_{\Omega}}$ (i.e., $0 \leqslant \xi_{\Omega} \leqslant \pi/2$) and $\hat{X}_{\Omega}(\Psi) = \cos \Psi_{\Omega} \, \hat{p}_{\Omega} - \sin \Psi_{\Omega} \, \hat{q}_{\Omega}$ is the generalized quadrature of mode Ω. The observables above represent a continuous change of modal basis dependent on the parameter ξ as the upper sideband is attenuated close to resonance (in fact, $\xi_{\Omega} \to 0$ for $\Delta \ll -\Omega/\gamma$ and $-\Omega/\gamma \ll \Delta \ll 0$). One may denote the new quadrature basis as $\hat{P}_{\xi_{\Omega}} = (\hat{p}_{-\Omega} + \cos \xi_{\Omega} \hat{X}_{\Omega}(\Psi))/\sin \xi_{\Omega}$ and $\hat{Q}_{\xi_{\Omega}} = (-\hat{q}_{-\Omega} + \cos \xi_{\Omega} \hat{X}_{\Omega}(\Psi - \pi/2))/\sin \xi_{\Omega}$. Phase coherent detection provides for each modal transformation above (fixed ξ) the possibility of observing any direction in its phase space, since the combination of cosine and sine photocurrent components yields in this case

$$\hat{J}_{\Theta} \approx \cos \Theta \sin \xi_{\Omega} \hat{P}_{\xi_{\Omega}} + \sin \Theta \sin \xi_{\Omega} \hat{Q}_{\xi_{\Omega}} + \sin \xi_{\Omega} \hat{u}'. \quad (17)$$

Hence region 1 sees the continuous transformation of measurement basis from $\mathcal{S}$ and $\mathcal{A}$ modes ($\hat{P}_{\xi_{\Omega}} \approx \hat{p}_s$ and $\hat{Q}_{\xi_{\Omega}} \approx \hat{q}_a$ for $\Delta \ll -\Omega/\gamma$) to a direct measurement of lower sideband

phase space at $\Delta = -\Omega/\gamma$ [Eq. (14)] and back to $\mathcal{S}$ and $\mathcal{A}$ modes in region 2 ($\Delta \approx 0$).

Similar considerations lead to the expressions of quantum measurements in region 3, with the upper sideband assuming the same prominent role that the lower sideband has in region 1. The quantum observables are obtained from Eqs. (15) and (16) by the exchange $\Omega \to -\Omega$. In particular, the phase space of upper sideband is measured when the cavity is at exact resonance with the lower sideband ($\Delta = \Omega/\gamma$), yielding a quantum measurement operator analogous to that of Eq. (14).

Resonator detection with the impedance-matched resonator thus accesses the two-mode quantum state by measuring it in two different single-mode basis: $\{\hat{p}_\Omega, \hat{q}_\Omega\}$ in region 1, $\{\hat{p}_s, \hat{q}_s\}$ and $\{\hat{p}_a, \hat{q}_a\}$ in region 2, and $\{\hat{p}_{-\Omega}, \hat{q}_{-\Omega}\}$ in region 3. All intermediate modal combinations are also available, according to Eqs. (15) and (16). The ability to observe single-mode phase spaces for different sets of modal basis in the two-mode space of sidebands allows RD to reconstruct the complete two-mode spectral quantum state. Although $d = 0$ represents an ideal scenario, realistic experimental conditions should consider technical noise on the detection circuit. The optimum situation to be pursued in a realistic experiment entails a minimization of d by a compromise between the ratio between the technical noise power and the quantum noise power of interest.

D. Two-mode quantum state reconstruction

The three detuning regions where the RD measurement operator presents different well defined behaviors in the simplifying scenario of a narrow linewidth resonator merge seamlessly in the actual measurement with a typical resonator, for which the condition $\gamma \ll \Omega$ is not necessarily satisfied. The complete expression for the general quantum observable of resonator detection with the impedance matched resonator is

$$\hat{J}_\Theta(\Delta) = \cos\xi_\Omega \, \hat{X}_\Omega(\theta) + \cos\xi_{-\Omega} \, \hat{X}_{-\Omega}(\theta')$$
$$+ \sin\xi_\Omega \, \hat{v}_\Omega + \sin\xi_{-\Omega} \, \hat{v}_{-\Omega}, \quad (18)$$

where $\theta = \Psi_0 - \Psi_\Omega + \Theta$ and $\theta' = \Psi_0 - \Psi_{-\Omega} - \Theta + \pi$. This measurement operator has the form of the complete two-mode operator of Eq. (6), although combined with additional vacuum contributions that preserve the commutation relations when substituting individual quantum modes by vacuum fields. Alternatively, the observables of resonator detection can also be written in terms of real functions of detuning defined by $R_{\pm\Omega}(\Delta) = x_{\pm\Omega}(\Delta) + i y_{\pm\Omega}(\Delta)$,

$$\hat{J}_{\cos} = x_\Omega \, \hat{p}_\Omega + y_\Omega \, \hat{q}_\Omega + x_{-\Omega} \, \hat{p}_{-\Omega} + y_{-\Omega} \, \hat{q}_{-\Omega} + \hat{w}_{\cos}, \quad (19)$$

$$\hat{J}_{\sin} = -y_\Omega \, \hat{p}_\Omega + x_\Omega \, \hat{q}_\Omega + y_{-\Omega} \, \hat{p}_{-\Omega} - x_{-\Omega} \, \hat{q}_{-\Omega} + \hat{w}_{\sin}, \quad (20)$$

a more convenient expression to perform numerical fitting to the experimental data. The vacuum operators are defined as $\hat{w}_{\cos} = \sqrt{T_\Omega} \, \hat{u}_\Omega + \sqrt{T_{-\Omega}} \, \hat{u}_{-\Omega}$ and $\hat{w}_{\sin} = \sqrt{T_\Omega} \, \hat{v}_\Omega + \sqrt{T_{-\Omega}} \, \hat{v}_{-\Omega}$. In the basis of $\mathcal{S}$ and $\mathcal{A}$ modes, these observables read as

$$\hat{J}_{\cos} = x_s \, \hat{p}_s + y_s \, \hat{q}_s + x_a \, \hat{p}_a + y_a \, \hat{q}_a + \hat{w}_{\cos}, \quad (21)$$

$$\hat{J}_{\sin} = -y_s \, \hat{p}_s + x_s \, \hat{q}_s + y_a \, \hat{p}_a - x_a \, \hat{q}_a + \hat{w}_{\sin}. \quad (22)$$

Figure 1 depicts the coefficients of quadrature operators in Eqs. (19)–(22) for a narrow linewidth resonator. It differs from the figures presented in Ref. [2], where we focused on the second order momenta associated to the covariance matrix under the assumption of stationary of the measurement, while here we are detailing the transformation of the field operators in an assumption-free treatment. The main features of resonator detection can be seen in the three different detuning regions separated in the figure by shaded backgrounds, as further discussed in Appendix A. The coefficients appearing in $\hat{J}_{\cos}$ and $\hat{J}_{\sin}$ are shown on two different modal basis as functions of cavity detuning. The resonator linewidth has been chosen as $\gamma = \Omega/20$ to allow a clear separation of detuning regions. The spectral basis of sideband modes (top row) is better suited to understand the quantum transformations in regions 1 ($\Delta < -10$) and 2 ($\Delta > 10$), where the individual sidebands undergo phase shift and attenuation. The $\mathcal{S}$ and $\mathcal{A}$ modal basis (bottom row) simplifies the description of region 2 ($-10 < \Delta < 10$), whereby it is clear that (just like in a homodyning measurement) the cosine component promotes a phase space rotation of the $\mathcal{S}$ mode, while the sine component rotates the phase space of the $\mathcal{A}$ mode.

As we have discussed, although we have, from Eqs. (19)–(22), the ability to recover the expected values of each quadrature on each mode from the measurement of either $\hat{J}_{\cos}$ or $\hat{J}_{\sin}$, these curves will not allow a complete reconstruction of the state. It will only be possible in the case of a lossy cavity. A more realistic situation should also include the effects of mode matching of the field with the resonator (Appendix B). Depicting the mode mismatch by f^2, the spectral photocurrent operator, previously given by Eq. (A5), becomes

$$\hat{J}_\Omega(\Delta) = G_\Omega^*(\Delta) \, \hat{a}_\Omega + G_{-\Omega}(\Delta) \, \hat{a}_{-\Omega}^\dagger + \hat{J}_v', \quad (23)$$

where

$$G_\Omega(\Delta) = (1 - f^2) |r(\Delta)| R_\Omega(\Delta) + f^2 \quad (24)$$

and the vacuum term is

$$\hat{J}_v' = f\sqrt{1 - f^2}[(1 - |r(\Delta)| R_\Omega^*)\hat{c}_\Omega + $$
$$+ (1 - |r(\Delta)| R_{-\Omega})\hat{c}_{-\Omega}^\dagger] + \sqrt{1 - f^2}|r(\Delta)|\hat{J}_v. \quad (25)$$

The observables of resonator detection with modal mismatch written in terms of spectral mode quadratures have the same form as in Eqs. (19) and (20) with the substitutions $x_\Omega \to x_\Omega'$ and $y_\Omega \to y_\Omega'$ defined as $G_\Omega(\Delta) = x_\Omega' + i y_\Omega'$. The vacuum terms are also substituted by the Hermitian and anti-Hermitian parts of Eq. (25). The main effect of modal contamination is to decrease the angular interval of phase space rotations, by removing redundant rotations in the ideal scenario of an impedance matched resonator ($d = 0$). For resonators in the intermediate scenario $0 < d < 1$, modal contamination can help the access to two-mode features of the Gaussian quantum state with better sensitivity.

In Fig. 2, we present the coefficients for $\hat{J}_{\cos}$ and $\hat{J}_{\sin}$ in the real scenario we are evaluating in this article: beatnote frequency $\Omega = 2.9\,\gamma$ is close to the resonator linewidth, the resonator is nearly impedance matched ($d = 0.05$), and a small mismatch for the spatial mode is taken in account ($f^2 = 0.15$). As we have seen, some impedance matching is
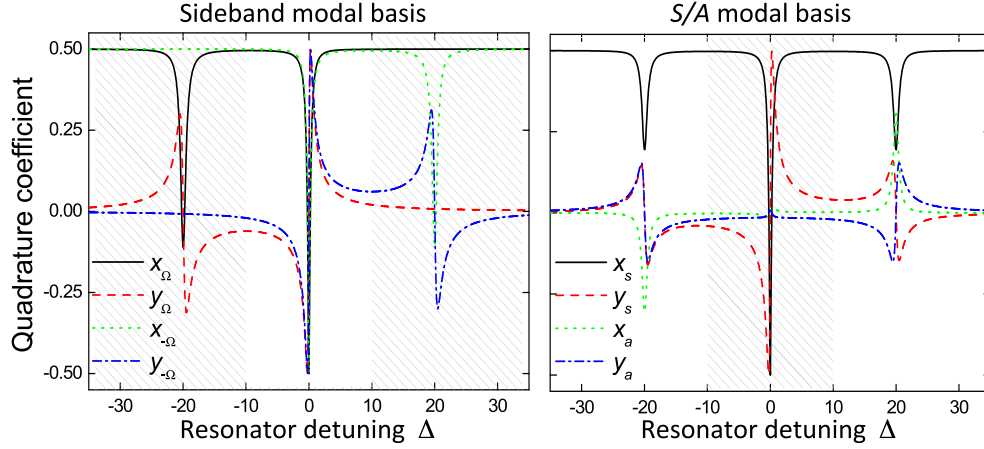
FIG. 1. Coefficients of resonator detection as functions of resonator detuning Δ. Sideband frequency is $\Omega = 20\gamma$. Left: Coefficients as written on the modal basis of spectral sidebands [Eqs. (19) and (20)]. The dashed regions show the phase space rotation of individual sideband modes. Right: Coefficients as written on the $\mathcal{S}$ and $\mathcal{A}$ modal basis [Eqs. (21) and (22)]. Phase space rotation of $\mathcal{S}$ and $\mathcal{A}$ modes occurs on the dashed region.

a *necessary* condition for the complete mapping of the four dimensional state.

III. QUANTUM MEASUREMENT OF TWO-MODE DISPLACED QUANTUM STATE

A. Encoding phase information in quantum states

Displacement of the vacuum field is probably the simplest conceptual quantum operation capable of producing quantum states with clear phase information. Luckily, the experimental generation of coherent states in spectral field modes is equally simple and clear. Here we present the use of RD in a phase-modulated laser beam as a proof-of-principle demonstration of phase coherent detection.

Let us then consider the *"phase modulation"* of an intense field by an electro-optical modulator (EOM). In this process, the refractive index of the EOM crystal is modified by an external electric field, creating a controllable phase

delay on the laser beam passing through the crystal. Therefore the classical electric field of light $E(t) = E_0 \exp[i(\omega_0 t + \beta)]$ oscillating at optical frequencies can be periodically delayed by a radio-frequency electric field producing a phase shift $\beta \rightarrow \beta(t) = 2\beta_0 \cos(\Omega t + \Phi)$. If the modulation amplitude is small enough ($\beta_0 \ll 2\pi$), the phase-modulated laser can be described by the electric field amplitude

$$E(t) \approx E_0 \, e^{i\omega_0 t} + iE_0\beta_0 \, e^{i\Phi} \, e^{i(\omega_0 + \Omega)t} + iE_0\beta_0 \, e^{-i\Phi} \, e^{i(\omega_0 - \Omega)t},$$
(26)

where higher frequency components can be disregarded. Thus we see from Eq. (26) that phase modulation is actually described in the quantum picture as the displacement of upper and lower sideband modes with coherent states possessing the amplitudes $\alpha_\Omega = iE_0\beta_0 \, e^{i\Phi}$ and $\alpha_{-\Omega} = -\alpha_\Omega^*$. The quantum state of sideband modes is Gaussian and separable, and equal to

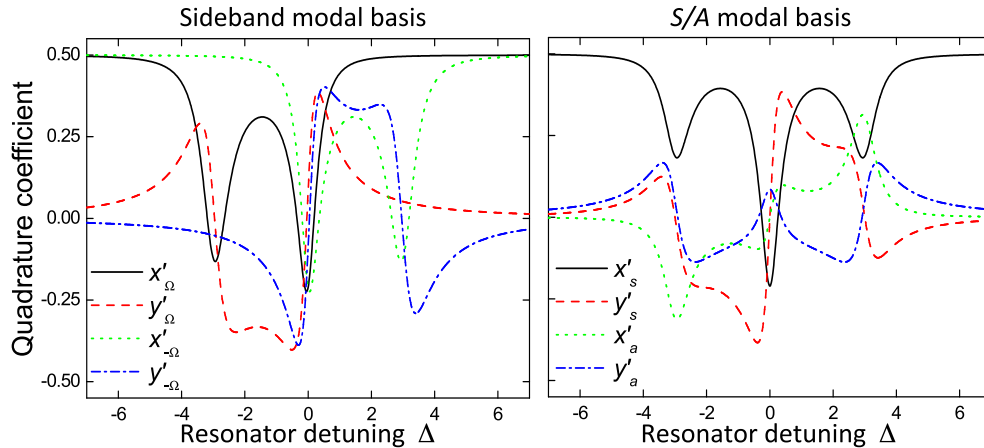$$|\psi\rangle = |\alpha_\Omega\rangle_\Omega \otimes |\alpha_{-\Omega}\rangle_{-\Omega}.$$
(27)

FIG. 2. Coefficients of resonator detection as functions of resonator detuning Δ. Line styles follow the same convention as in Fig. 1. Parameters are: $\Omega = 2.9\gamma$ $d = 0.05$, and $f^2 = 0.15$. They represent the realistic conditions at which the experiments of Sec. III have been performed.

The motivation for the name 'phase modulation' is made clear in the semi-classical interpretation of quantum noise [2]. In this picture, valid as long as second-order moments (sufficient to describe Gaussian states) are concerned, 'effective' quadrature operators can be found to succintly describe the photocurrent spectral noise power by using only half the number of actual field modes. The semi-classical amplitude and phase quadrature operators, respectively defined as $\hat{\mathcal{P}}_\Omega = \hat{a}_\Omega + \hat{a}^\dagger_{-\Omega}$ and $\hat{\mathcal{Q}}_\Omega = -i(\hat{a}_\Omega - \hat{a}^\dagger_{-\Omega})$, yield over the quantum state of Eq. (27) the mean amplitudes

$$\langle \hat{\mathcal{P}}_\Omega \rangle = 0 \quad \text{and} \quad \langle \hat{\mathcal{Q}}_\Omega \rangle = 2E_0\beta_0\, e^{i\Phi}, \tag{28}$$

i.e., only the semiclassical phase quadrature is displaced, thereby justifying the nomenclature. In terms of *bona fide* quadrature observables of spectral modes, the semi-classical quadratures read as

$$\hat{\mathcal{P}}_\Omega = \hat{p}_s + i\hat{q}_a, \qquad \hat{\mathcal{Q}}_\Omega = \hat{q}_s - i\hat{p}_a. \tag{29}$$

Hence Eq. (28) furnishes the quantum state averages of sideband modes quadrature observables as

$$\frac{1}{\sqrt{2}}\langle \hat{p}_\Omega + \hat{p}_{-\Omega} \rangle = 0, \qquad \frac{1}{\sqrt{2}}\langle \hat{q}_\Omega + \hat{q}_{-\Omega} \rangle = s\cos\Phi, \tag{30}$$

$$\frac{1}{\sqrt{2}}\langle \hat{q}_\Omega - \hat{q}_{-\Omega} \rangle = 0, \qquad \frac{1}{\sqrt{2}}\langle \hat{p}_\Omega - \hat{p}_{-\Omega} \rangle = s\sin\Phi, \tag{31}$$

where $s = \sqrt{2}\,|\alpha_\Omega| = \sqrt{2}\,E_0\beta_0$.

For an ideal EOM supposed not to include technical noise on the sideband modes, the conditions above correspond to the generation of two classically correlated coherent quantum states. One coherent state results from the displacement of the phase quadrature of $\mathcal{S}$ mode [Eq. (31)] and the other stems from the amplitude displacement of $\mathcal{A}$ mode [Eq. (31)]. On this modal basis, the phase Φ of phase modulation only determines the amplitude of the displacements on fixed directions, since the quantum state then reads as

$$|\psi\rangle = |\alpha_s\rangle_s \otimes |\alpha_a\rangle_a, \tag{32}$$

where $\alpha_s = is\cos\Phi$ and $\alpha_a = s\sin\Phi$.

Therefore the semiclassical terminology of phase modulation corresponds, in the formal quantum treatment of field modes, to the generation of simultaneous spectral sideband displacements with complex conjugated amplitudes (i.e., single-mode phases *and amplitudes* are actually displaced), as can be seen in Fig. 3. Although they are not quantum correlated, since each mode is shot noise limited, they present classical correlations due to their conjugated displacement phases.

To access the phase information of the quantum state of Eq. (27) in the experiment, phase coherent RD requires a well-defined relative phase between the generated spectral quantum state and the measured spectral photocurrent component. We achieve this regime by utilizing the *same electronic reference* to generate and measure the spectral sideband modes [21], a situation completely analogous to the usual practice of utilizing the *same laser* to produce the quantum state and homodyne it.

B. Experimental setup

In our experiment, the two-mode spectral quantum state is generated by an EOM (fed by the eLO) acting on the laser
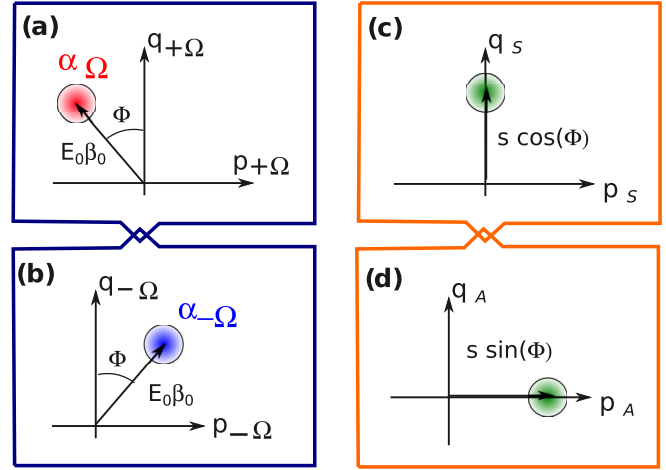

FIG. 3. Two-mode quantum state produced by acting upon a laser beam with an EOM. Insets (a) and (b) depict the quantum state in the modal basis of sidebands. The quantum state is represented in the modal basis of symmetric $\mathcal{S}$ and antisymmetric $\mathcal{A}$ modal basis in insets (c) and (b).

beam, in this manner performing the displacement quantum operation on both sideband modes. The displacement amplitudes are proportional to the eLO amplitude, while their phases are defined with respect to the eLO phase. On the measurement side, the laser beam plays the role of the LO field with respect to which RD delays and attenuates the sideband modes, while the eLO becomes the electronic reference, with fixed amplitude and phase, with respect to which spectral photocurrent components are defined. Since the phase of the spectral coherent states depend both on the LO and the eLO phases, we ensure that good phase relations exist in the two 'downmixing' processes involved in resonator detection: first, the *optical* downmixing between LO and sidebands quantum state ensures good reference exists to define amplitude and phase *quadratures* in phase space; second, the *electronic* downmixing between the photocurrent and the eLO allows us to define *cosine and sine* spectral components (this step is not pursued in experiments with quantum noise). The reason why the phase diffusion between LO and eLO factors out in our quantum measurement stems from the fact that the only phases that matter to our signal concern the quantum state: as long as it is coherent with both LO and eLO at the same time, the quantum measurement occurs in a phase coherent regime. A related situation is very common in experiments in quantum optics: by optical phase one usually means the phase of a light beam with respect to itself in a different time or position—the absolute phase is irrelevant. Our setup makes the absolute phase of both the optical LO and the eLO irrelevant at the same time, making it unnecessary to lock their phases together.

With such arrangement, we are able to produce different quantum states by either changing the eLO amplitude or the relative phase between the fraction of eLO fed to the EOM and the fraction of it sent to spectral analysis. In changing the phase, it is also correct to say that we produce the same quantum state, but vary the spectral component being measured (equivalent to varying Θ). Here we adopt the first
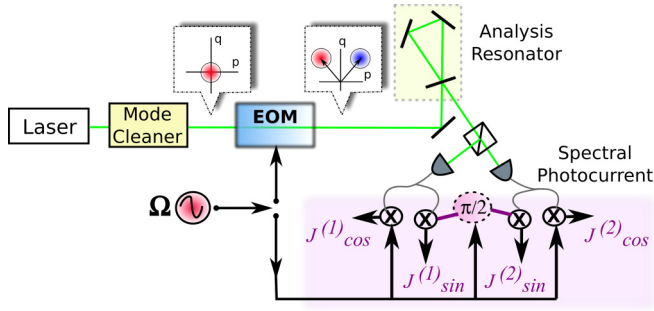
FIG. 4. Experimental setup. The laser beam is modulated by the EOM and coupled to an optical cavity for resonator detection. The reflected beam is measured by two photodetectors to provide the quantum noise and the SQL simultaneously. The spectral analysis of the photocurrent signals is performed using the same electronic reference used to drive the EOM and hence produce the quantum state, in this manner achieving phase-locked detection. Sine and cosine photocurrent components are individually sampled and recorded by an acquisition board.

interpretation, so as to keep the quantum measurement fixed and the quantum state tunable.

The laser system is comprised of a frequency-doubled diode-pumped Nd:YAG laser at 532 nm (Innolight Diabolo) and spectrally filtered by an optical resonator to achieve shot noise limited spectral sideband modes (vacuum) at the intended analysis frequency as depicted in Fig. 4. The sideband quantum state is produced by 'phase modulation' with an electro-optical modulator (EOM) at $\Omega/(2\pi) = 17$ MHz. Resonator detection is performed by employing an optical cavity with 5.9(3) MHz resonance bandwith [$\Omega/\gamma = 2.9(2)$] and impedance matching parameter given by $d = 0.05$. Spatial mode matching achieves 86% coupling ($f^2 = 0.15$) with the TEM$_{00}$ Hermite-Gaussian mode (scanned mode). Although this value could be easily made very close to 100% in our experiment (typically >99.5%), we noticed empirically that lower values of spatial matching would provide better access to two-mode features of the quantum state in our particular situation, a conclusion completely ractified by the model of Eq. (23). The reflection of the Analysis resonator is divided by a beam splitter and sent to a pair of photodetectors, allowing the use of vacuum homodyning for precise calibration of the standard quantum level along the measurement.

Photodetection is realized by two amplified detectors with 25 MHz bandwidth. Each photodetector separates the photodiode photocurrent by frequency: the transmission of a low-pass filter with 10-kHz cutoff frequency samples the beam mean intensity (DC signal), while the selected high-frequency components from 10 kHz up to 30 MHz (HF signal) yield the experimental signal of interest displaying quantum features. One spectral component is selected from the temporal signal by downmixing it with the use of an electronic local oscillator (eLO) with frequency Ω (Fig. 4) and filtering the result in low-pass with 300 kHz cutoff frequency (i.e., 600 kHz full width).

The two electronic downmixing components (cosine and sine, or, equivalently, in-phase and in-quadrature with respect to the eLO) of each detector are recorded by an A/D converter
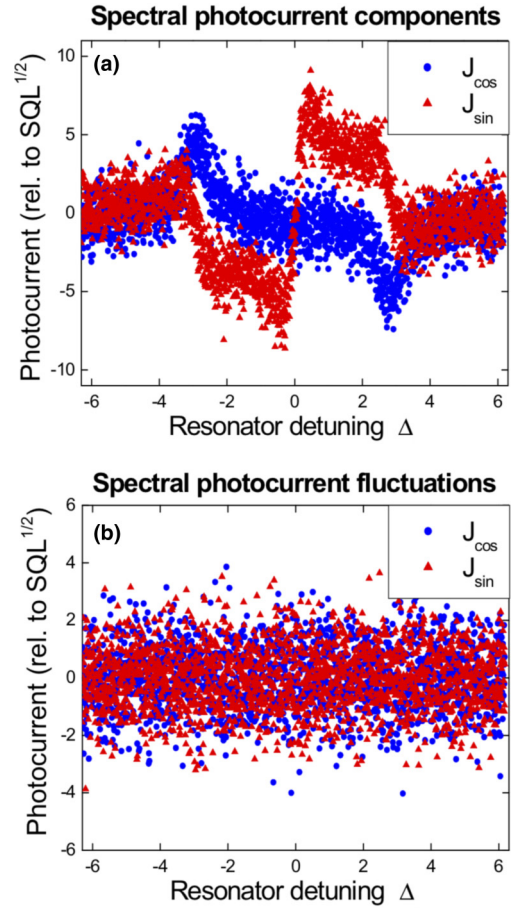

FIG. 5. Spectral components of the photocurrent as functions of resonator detuning Δ. Each data point corresponds to the realization of a quantum measurement of either $\hat{J}_{\cos}$ (blue cicles) or $\hat{J}_{\sin}$ (red triangles). (a) Raw data normalized to the square root of the SQL. (b) Quantum fluctuations appearing on the data on top (i.e., mean values have been subtracted). Each figure shows a sample of 2000 data points from the original 450 000 quantum measurements in each curve.

connected to a computer. Data acquisition rate is 600 kHz to produce independent quantum measurements. The subtraction of demodulated HF components stemming from the two photodetectors provides the SQL, and their sum is further analyzed, giving rise to the spectral photocurrent components. Quantum state reconstruction is realized by scanning the cavity length with a piezoelectric element holding one of the cavity mirrors. Cavity resonance frequency is thus scanned through the spectral modes of interest. Each scan takes 0.75 s and collects 450 000 quantum measurements of each spectral photocurrent component.

C. Experimental results

Figure 5(a) presents the set of individual quantum measurements (normalized to the SQL) of the phase modulated laser obtained with RD as function of resonator detuning. The phase coherent nature of the quantum measurement guarantees that the cosine ($\hat{J}_{\cos}$) and sine ($\hat{J}_{\cos}$) components are truly accessing specific marginal distributions of the two-mode
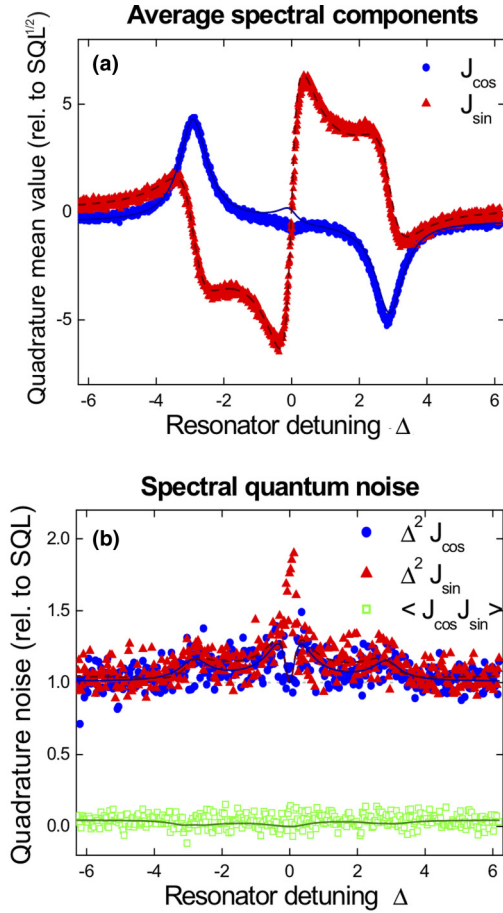
FIG. 6. Moments of the cosine and sine photocurrent components of Fig. 5 corresponding to the quantum measurement operators $\hat{J}_{\cos}$ and $\hat{J}_{\sin}$ [Eq. (23)]. (a) First-order moments $\langle \hat{J}_{\cos} \rangle$ (blue circles) and $\langle \hat{J}_{\sin} \rangle$ (red triangles). (b) Second-order moments $\Delta^2 \hat{J}_{\cos}$ (blue circles), $\Delta^2 \hat{J}_{\sin}$ (red triangles), and $\langle \hat{J}_{\cos} \hat{J}_{\sin} \rangle$ (green squares). Curve fits involving the measurement operator model of Eq. (23) are depicted by solid and dashed lines on top of the respective data set.

quantum state Wigner function as the resonator detuning Δ is varied. In fact, the signal shows not only the usual quantum fluctuations around the null value [2], but also the mean values of spectral components at each detuning. Figure 5(b) complements the picture by isolating the fluctuations of Fig. 5(a) obtained by subtracting from each quantum measurement the mean value of 200 data points around it, acting therefore as a high-pass filter. This step in the analysis is not necessary, but facilitates the separate visualization of first- and second-order photocurrent moments.

We extract information from the data in Fig. 5 in two steps. Firstly, we address the photocurrent mean values $\langle \hat{J}_{\cos} \rangle$ and $\langle \hat{J}_{\sin} \rangle$ calculated over 200 individual quantum measurements, yielding curves with 22 500 values of detuning. Those curves are presented in Fig. 6(a) and provide information on the quadrature operator mean values $\langle \hat{p}_{\pm\Omega} \rangle$ and $\langle \hat{q}_{\pm\Omega} \rangle$ by fitting (solid and dashed lines) the quantum state average of the measurement operator of Eq. (23). As can be noticed, this mean value is precisely the kind of error curve obtained in the Pound-Drever-Hall technique for stabilizing a cavity [31]. Secondly, we calculate from Fig. 5(b) the second-order

photocurrent moments—variances $\Delta^2 \hat{J}_{\cos}$ and $\Delta^2 \hat{J}_{\sin}$ and the correlation $\langle \hat{J}_{\cos} \hat{J}_{\sin} \rangle$—to extract the covariance matrix of the two-mode Gaussian quantum state. The elements of the covariance matrix are obtained by fitting the quantum state average of the square of the measurement operator of Eq. (23), a result presented in Fig. 6(b) by the solid and dashed lines.

To perform the aforementioned RD model curve fits, we first obtain the general shapes of the curves $G_{\pm\Omega}$ as functions of Δ (depicted in Fig. 2). The DC signal of the photocurrent provides the resonator parameter d as well as the scaling factor that allows us to calibrate the Δ axis (we note that Δ is defined relative to the resonator bandwidth). The quadrature operator moments appear in the data fitting as coefficients to the real and imaginary parts of the curves $G_{\pm\Omega}(\Delta)$. In this manner, the first-order moments [Fig. 6(a)] of the measured photocurrent (Fig. 5) can be understood (in the context of the curve fitting used to extract quadrature operator moments) as a sum of the curves depicted in Fig. 2 weighted by the first-order moments of field quadrature operators. The same reasoning applies to the second-order moment curve fittings in Fig. 6(b).

Although in our experiment the RD is not in the narrow resonator limit $\gamma \ll \Omega$, but rather presents $\gamma \approx \Omega/3$, it is still possible to understand Fig. 6(a) qualitatively. The detuning region close to LO resonance ($\Delta \approx 0$) can be seen to reveal features in the $\mathcal{S}/\mathcal{A}$ modal basis by comparing the data profiles with the expected quantum state averages of Eq. (31). In fact, the $\langle \hat{J}_{\cos} \rangle$ curve indicates that $\hat{p}_s \approx \hat{q}_s \approx 0$, while the curve for $\langle \hat{J}_{\sin} \rangle$ points at the existence of some displaced state in mode $\mathcal{A}$. Similarly, the detuning regions where the optical resonator is nearly resonant with one of the sidebands, at $\Delta \approx \pm\Omega/\gamma \approx \pm3$, indicate that both sideband modes $\pm\Omega$ are displaced by the same amount, since the curves are symmetric, essentially showing the same features for positive and negative detuning expected from Eq. (27). The quantitative analysis obtained by the curve fits, represented by solid lines in Fig. 6(a), attest that this is indeed the case. On the modal $\mathcal{S}/\mathcal{A}$ basis, we obtain the first-order quadrature operator moments $\langle \hat{p}_s \rangle = -0.6(7)$, $\langle \hat{q}_s \rangle = 2.2(5)$, $\langle \hat{p}_a \rangle = 11.8(7)$, and $\langle \hat{q}_a \rangle = 0.2(5)$. We note that these numbers are measured relatively to the scale determined by the SQL in phase space (i.e., the value 1 would indicate a coherent state displaced by the standard deviation of its Gaussian probability distribution). On the spectral basis of sideband modes, we obtain $\langle \hat{p}_\Omega \rangle = -8.8(7)$, $\langle \hat{q}_\Omega \rangle = 1.7(5)$, $\langle \hat{p}_{-\Omega} \rangle = 7.9(7)$, and $\langle \hat{q}_{-\Omega} \rangle = 1.4(5)$, whereby it is clear that sideband modes are displaced by equal amplitudes (given the experimental uncertainty) in symmetric directions in phase space, as expected by the quantum model of phase modulation described in Fig. 3, with with $s = \sqrt{2}E_0\beta_0 = 12.0(9)$ and $\theta = 1.38(5)$ rad.

We note that the usual phase mixed detection would erase phase information encoded in the first order moments, completely nullifying them and artificially increasing the second-order moments to erroneously identify the phase modulated laser as possessing excess (semi-classical) phase noise. The two-mode sideband quantum state would then appear to show zero quadrature average and balanced excess noise: essentially, a thermal state [1]. Measurement mixedness would in this case be completely transferred to a perceived lack of purity of the quantum state (since the thermal state has the lowest degree of purity for a given temperature). Phase

information allows us to perform a pure measurement and hence show that the quantum state is very close to a coherent state in the sideband modes: a situation very different from the inherent classical randomness of a thermal state.

Figure 6(b) depicts the experimental results regarding the photocurrent noise power and its interpretation in terms of the Gaussian quantum state covariance matrix. Three possible experimental combinations are possible: $\Delta^2 \hat{J}_{\cos} = \langle(\hat{J}_{\cos} - \langle \hat{J}_{\cos}\rangle)^2\rangle$, $\Delta^2 \hat{J}_{\sin} = \langle(\hat{J}_{\sin} - \langle \hat{J}_{\sin}\rangle)^2\rangle$, and $\langle(\hat{J}_{\cos} - \langle \hat{J}_{\cos}\rangle)(\hat{J}_{\sin} - \langle \hat{J}_{\sin}\rangle)\rangle$, respectively corresponding to the spectral noise power of photocurrent cosine and sine components, and to the correlation between those components. Variances and correlations are calculated over groups of 1000 quantum measurements, and hence one resonator scan is composed of 450 detuning values. Curve fits to the data, shown on top of the respective data set, involve the square of the measurement operator of Eq. (23). Similarly to the reasoning presented in the analysis of Fig. 6(A), we may regard $\Delta \hat{J}_{\cos}$, $\Delta \hat{J}_{\sin}$ and $\langle \hat{J}_{\cos}\hat{J}_{\sin}\rangle$ as sums of curves taken as functions of Δ weighted by elements of the covariance matrix. For instance, the coefficient of $\Delta^2 \hat{p}_\Omega$ is, according to Eq. (23), given by $x_\Omega^2(\Delta) = \text{Re}\{G_\Omega^*\}^2$, a function of Δ given by the square of the black solid curve on the top row of Fig. (2). In fact, the coefficients of the quadrature operator variances $\Delta^2 \hat{p}_{\pm\Omega}$ and $\Delta^2 \hat{q}_{\pm\Omega}$ are given by the square of the functions of Δ seen in Fig. (2), respectively $x_{\pm\Omega}(\Delta)$ and $y_{\pm\Omega}(\Delta)$. Correlations between different quadrature operators contribute to the noise curves of Fig. 6(b) as products of the respective functions of Δ, as expected. Given the generally asymmetric shapes of those coefficients, it is clear that the data in Fig. 5(b) favors symmetric noise in modes $\pm\Omega$. Furthermore, all noise terms are nearly shot-noise limited. The quantitative analysis performed by the curve fittings yield the spectral operator moments $\Delta^2 \hat{p}_\Omega = \Delta^2 \hat{q}_{-\Omega} = 1.25(3)$ and $\Delta^2 \hat{q}_\Omega = \Delta^2 \hat{p}_{-\Omega} = 1.28(3)$, showing that the sideband quantum states are not exactly coherent states, but rather present slight excess (classical) noise. These results indicate that the EOM introduces a small amount of balanced thermal noise in the sideband modes, that can be originated from Johnson noise of the driving electronics. According to the data fit, the energy imbalance is proportional to $\langle \hat{J}_{\cos}\hat{J}_{\sin}\rangle = (\Delta^2 \hat{p}_\Omega + \Delta^2 \hat{q}_\Omega) - (\Delta^2 \hat{p}_{-\Omega} + \Delta^2 \hat{q}_{-\Omega}) = -0.01(3)$, hence compatible with zero. In the basis of $\mathcal{S}$ and $\mathcal{A}$ modes, the EOM produces classical noise in the quadratures $\Delta^2 \hat{q}_+ = 1.50(3)$ and $\Delta^2 \hat{p}_- = 1.03(3)$. According to Eq. (31), that would be interpreted in the semi-classical picture as a slight addition of 'phase' noise to the laser beam.

Putting together the first- and second-order moments obtained with RD, the experimental curve of Fig. 6(a) can be understood as the two-mode rotation of the coherent state displaced by the EOM "smeared" by (roughly) the shot noise inherent to the Heisenberg uncertainty principle.

The ability to control the phase of the two-mode displaced quantum state is demonstrated in Fig. 7. We have produced 14 different coherent quantum states by changing the displacement phase Φ fed to the EOM. For each value of Φ, we obtain experimental curves analogous to those of Fig. 6(a), to which we perform model fits to acquire the values of $\langle \hat{p}_{\pm\Omega}\rangle$ and $\langle \hat{q}_{\pm\Omega}\rangle$ or, by a change of modal basis, the moments $\langle \hat{p}_s\rangle$, $\langle \hat{q}_s\rangle$, $\langle \hat{p}_a\rangle$, and $\langle \hat{q}_a\rangle$. Figure 7 presents the first-order moments in the modal basis $\mathcal{S}$ and $\mathcal{A}$ due to their increased simplicity
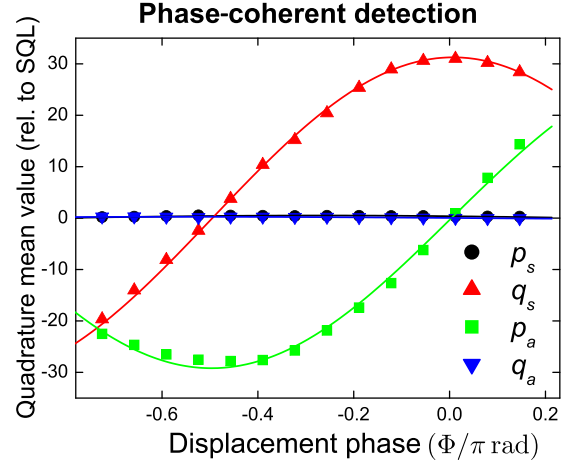

FIG. 7. Two-mode coherent state in modes $\mathcal{S}$ and $\mathcal{A}$ produced by varying the phase Φ of EOM modulation [Eq. (31)]. In particular, the quadratures $\hat{p}_s$ and $\hat{q}_a$ show null displacement for all values of Φ. The lines are fits of sinusoidal functions, consistently matching the experimental results.

[Eq. (31)] as the displacement phase Φ is varied. All quantum states are compatible with simple phase space rotations of the displacement values $\langle \hat{p}_s\rangle = -0.5(1)$, $\langle \hat{q}_s\rangle = 31.3(5)$, $\langle \hat{p}_a\rangle = 29.2(5)$, and $\langle \hat{q}_a\rangle = -0.1(3)$.

IV. CONCLUSION

The measurement technique of RD grants access to "hidden" sectors of the two-mode phase space of the spectral quantum state by providing modal-dependent attenuation and phase delay with the aid of a controllable optical resonance, even in the usual situation of a phase-mixed measurement [1]. While the measurement then performed could be considered complete under the assumption of stationarity, it was yet restricted to the observation of a specific class of states.

In order to provide a *pure* measurement operator, phase coherent detection of the spectral photocurrent must be performed. We have shown that RD becomes in this case also an *assumption free complete* measurement technique, providing access to any direction of observation in the four-mode phase space where the Wigner function describes the quantum state—a fundamental condition to formally perform quantum state reconstruction of spectral modes. Phase coherent detection allows one to formally associate the photocurrent statistics with the probability distributions of *bona fide* modal quadrature observables, in this manner bringing the prospect of assumption-free quantum state reconstruction.

Phase coherent detection requires the existence of good phase relation between the quantum state and the local oscillators used as references (both in the optical and electronic downmixing processes). We demonstrate phase coherent RD by measuring a simple quantum state possessing the desired phase information, a displaced two-mode quantum state. We keep track of the phase coherence between the quantum state and the quantum observable by employing the laser beam and the EOM electronic modulation signal as *simultaneous* references. In this manner, we are able to recover the displacement phases of the two-mode quantum state. By coherently measuring the two (cosine and sine) spectral photocurrent

components, we have demonstrated the capability to obtain the complete two-mode quantum state in phase space. The technique in principle works for any quantum state, even those presenting non-Gaussian statistics. Furthermore, if combined with the developments of parametric detection, as shown in Ref. [10], it can provide a powerful broadband tool for state reconstruction.

In most experimental situations producing quantum states of the field, a weak seed beam, generated by an EOM, should suffice to introduce the necessary phase reference in the quantum state in order to later recover it in the measurement process. Alternatively, one could employ as optical LO laser beams showing spectral linewidth compatible with the inverse of the time needed to perform the full tomographic reconstruction of the quantum state [30]. Those procedures would introduce the missing degree of rigor in experiments aiming to arbitrarily manipulate the quadrature observables of spectral modes of the field. Using the electronic seed as a 'reference to itself' in the measurement process in the spectral domain is akin to the usual procedure of employing the laser beam as the "optical reference oscillator to itself" in order to keep track of the optical phase reference. As we show here, the same care must be exercised when performing the spectral analysis of the photocurrent fluctuations: leaving the spectral phase free leads to the onset of mixed quadrature measurements, a clear limitation for the implementation of quantum information protocols requiring formal pure measurement operators and quantum feedback. Resonator detection adds to those capabilities by offering a complete measurement of the two-mode spectral field quantum state in a alternative phase coherent regime.

APPENDIX A: RESONATOR DETECTION MEASUREMENT OPERATOR

For the sake of completeness, we present here a detailed analysis of the transformation of the field operator by the detuned cavity, as described initially in Ref. [2].

The field transformations taking place in RD are best described on the spectral modal basis. A high-finesse optical resonance centered at frequency ω_c with bandwidth 2γ performs in reflecting each spectral field mode the quantum operation

$$\hat{a}_\omega^{\text{out}} = r(\Delta_\omega)\,\hat{a}_\omega + t(\Delta_\omega)\,\hat{b}_\omega, \qquad (A1)$$

where $\hat{a}_\omega$ is the annihilation operation of the field of interest impinging on the resonator and $\hat{b}_\omega$ represents the modes in vacuum state transmitted by the resonator. The reflection $r(\Delta_\omega)$ and transmission $t(\Delta_\omega)$ coefficients are functions of the dimensionless detuning $\Delta_\omega = (\omega - \omega_c)/\gamma$. The measured

output field $\hat{a}_\omega^{\text{out}}$ is hence a combination of the spectral mode of interest and vacuum, after the first is attenuated and phase shifted by the amount

$$r(\Delta_\omega) \approx -\frac{\sqrt{d} + i\Delta_\omega}{1 - i\Delta_\omega} = \sqrt{1 - T(\Delta_\omega)}\,e^{i\Psi(\Delta_\omega)}. \qquad (A2)$$

This expression holds in the high finesse limit, as far as the input coupler is the main loss of the cavity. Here d is the *impedance matching parameter* (a fixed property of the optical resonator) and represents the fraction of light intensity reflected at exact resonance. For an impedance-matched resonator, light is completely transmitted at resonance (i.e., $d = 0$ and $|r(0)| = 0$), whereas for a lossless resonator light is totally reflected (i.e., $d = 1$ and $|r(\Delta_\omega)| = 1, \forall \Delta_\omega$). The spectral attenuation $T(\Delta_\omega)$ and phase shift $\Psi(\Delta_\omega)$ follow the explicit expressions:

$$T(\Delta_\omega) = \frac{1 - d}{1 + \Delta_\omega^2}, \qquad (A3)$$

$$\Psi(\Delta_\omega) = \arctan(\Delta) + \arctan(\Delta/\sqrt{d}). \qquad (A4)$$

Quantum state reconstruction requires scanning the optical resonance to sequentially transform according to Eq. (A1) the lower sideband, LO, and the upper sideband just prior to photodetection. The simplest transformation occurs for the LO mode: its mean amplitude α is attenuated and phase-shifted as $\alpha^{\text{out}} = r(\Delta)\alpha$, since the vacuum has null mean amplitude, where $\Delta = (\omega_0 - \omega_c)/\gamma$ is the detuning between LO and optical cavity. It is convenient to refer the other optical frequencies to the LO mode, thus we write Δ_ω as a function of the LO detuning as $\Delta_\omega = \Delta + \Omega/\gamma$ Applying these considerations to the transformations of Eq. (A1), the photodetection operator of Eq. (1) yields the spectral photocurrent operator of RD as

$$\hat{J}_\Omega(\Delta) = R_\Omega^*(\Delta)\,\hat{a}_\Omega + R_{-\Omega}(\Delta)\,\hat{a}_{-\Omega}^\dagger + \hat{J}_v, \qquad (A5)$$

where the notation has been simplified in $\hat{a}_{\omega_0 \pm \Omega} \to \hat{a}_{\pm\Omega}$, $\hat{J}_v$ stands for contribution of vacuum modes, and the transformation coefficients are

$$R_\Omega(\Delta) = e^{i\Psi(\Delta)}\,r^*(\Delta + \Omega/\gamma)$$
$$= \sqrt{1 - T(\Delta + \Omega/\gamma)}\,\exp\left[i\Psi(\Delta) - i\Psi(\Delta + \Omega/\gamma)\right].$$
$$(A6)$$

The three distinct spectral regions of the field (lower sideband, LO, and upper sideband) are simultaneously transformed by $R_\Omega(\Delta)$ as the cavity resonance frequency is scanned during quantum state reconstruction. Let us suppose for simplicity that sideband modes are separated by a frequency interval $\Omega \gg \gamma$ from the LO (i.e., narrow linewidth resonator), so that the transformations affecting each region of detuning do not interfere with one another. In this case, when the optical resonator is nearly resonant with the upper sideband ($\Delta \approx -\Omega/\gamma$), here called region 1, Eq. (A5) has off-resonant terms $e^{i\Psi(\Delta)} \approx 1$ and $r(\Delta - \Omega/\gamma) \approx 1$, so that the spectral photocurrent operator simplifies to

$$\hat{J}_\Omega(\Delta) \approx \sqrt{1 - T(\Delta + \Omega/\gamma)}\,e^{i\Psi(\Delta + \Omega/\gamma)}\,\hat{a}_\Omega + \hat{a}_{-\Omega}^\dagger$$
$$+ \sqrt{T(\Delta + \Omega/\gamma)}\,\hat{b}_\Omega. \qquad (A7)$$

The resonator detuning controls in this case the partial *substitution* of the upper sideband mode by the vacuum field and at the same time the *rotation* of its quasiprobability distribution by the angle $\Psi(\Delta + \Omega/\gamma)$. We note that the vacuum annihilation operator $\hat{b}_\Omega$ has been redefined to incorporate the phase rotation term in order to simplify the expression (we will employ this procedure wherever it is possible).

The second spectral region has the LO field interacting with the optical resonator ($\Delta \approx 0$), so that the off-resonant terms affecting the sidebands are $r(\Delta \pm \Omega/\gamma) \approx 1$ and the spectral operator reads as

$$\hat{J}_\Omega(\Delta) \approx \sqrt{1 - T(\Delta)}\big(e^{-i\Psi(\Delta)}\hat{a}_\Omega + e^{i\Psi(\Delta)}\hat{a}_{-\Omega}^\dagger\big). \quad \text{(A8)}$$

Hence apart from the attenuation factor $1 - T(\Delta)$ which changes the absolute power of the spectral noise and results in a redefinition of the standard quantum level (SQL) of the shot noise, in region 2 the joint phase space of the two spectral modes undergoes phase rotation *equivalent* to the transformation of spectral HD, i.e., in the $\mathcal{S}/\mathcal{A}$ modal basis. In this sense, resonator detection *contains* homodyne detection as part of the modal transformations leading to the measurement operator.

Spectral region 3 sees the transformation of Eq. (A7) applied to the lower sideband ($\Delta \approx \Omega/\gamma$). Explicitly, the spectral photocurrent operator in this region reads as

$$\hat{J}_\Omega(\Delta) \approx \hat{a}_\Omega + \sqrt{1 - T(\Delta - \Omega/\gamma)}\, e^{-i\Psi(\Delta - \Omega/\gamma)}\hat{a}_{-\Omega}^\dagger$$
$$+ \sqrt{T(\Delta - \Omega/\gamma)}\,\hat{b}_{-\Omega}^\dagger. \quad \text{(A9)}$$

The lower sideband mode undergoes transformations equivalent to those experienced by the upper sideband in region 1 as the detuning is varied.

Since the measurement operator in region 2 essentially mimics HD, the different features of RD must be present in regions 1 and 3. The exact effect on quantum noise of the special quantum transformations in those regions 1 and 3 strongly depends on the impedance matching parameter d. Resonator detection has two independent scenarios of interest, determined by the extreme values of d. In the first scenario, a lossless ideal resonator ($d = 1$) will have the sole effect of dephasing the spectral modes, i.e., no modal attenuation occurs. The spectral photocurrent operator then takes essentially the same form in regions 1, 2 and 3. For instance, in region 1 the operator becomes

$$\hat{J}_\Omega^{(1)}(\Delta) \approx e^{i\Psi(\Delta + \Omega/\gamma)/2}\big(e^{i\Psi(\Delta + \Omega/\gamma)/2}\hat{a}_\Omega$$
$$+ e^{-i\Psi(\Delta + \Omega/\gamma)/2}\hat{a}_{-\Omega}^\dagger\big), \quad \text{(A10)}$$

which has the same form of Eq. (A8) although with the opposite direction of rotation in phase space (the leading phase has no effect in measurement results). The same expression is valid for region 3 by simply changing the sign of the leading phase. Hence the three detuning regions implied by the lossless resonator do not differ from one another in the form of the measurement operator: RD becomes solely based on modal phase shifts and thus completely equivalent to spectral HD.

Different features regarding quantum state reconstruction appear in the second extreme scenario. The impedance-matched resonator ($d = 0$) substitutes the spectral mode at

exact resonance by another at the vacuum state. In the special case of region 2, this effect comes with no consequences, as attenuation of the LO mode simply decreases the amplification of sideband quantum noise provided by the LO. Around zero detuning, LO attenuation implies a recalibration of the SQL. Total attenuation of the LO would occur in the ideal case $d = 0$, meaning that technical noise would dominate the spectral photocurrent at $\Delta \approx 0$. In reality, this effect limits the minimum value of d in experiment by the smallest intensity at exact resonance still producing quantum noise with the desired signal-to-noise ratio.

In fact, modal substitution brings conceptual advantages when sideband modes are attenuated in regions 1 and 3. RD then provides direct measurements of individual sideband modes, in the same spirit of Eq. (3). For the special value of detuning $\Delta = -\Omega/\gamma$, one has $T(\Delta + \Omega/\gamma) = 1$, and Eq. (A9) yields

$$\hat{J}_\Omega(-\Omega/\gamma) = \hat{a}_{-\Omega}^\dagger + \hat{b}_\Omega, \quad \text{(A11)}$$

i.e., a measurement of the lower sideband mode (contaminated by vacuum noise). A similar relation is obtained for Eq. (4) at the detuning $\Delta = \Omega/\gamma$, and a direct measurement of upper sideband mode follows. We note that contamination of the field mode by vacuum is in fact common in tomographic reconstruction, brought by every type of modal contamination occurring in a realistic experiment. The information of the state is immediately recovered by deconvolution of the measured probability distribution with the calibrated vacuum distribution.

APPENDIX B: MODAL CONTAMINATION

The most relevant effect to cause deviations in the RD measurement operator effectively obtained in the laboratory from the ideal model lies in the possible spatial mode mismatch with the resonator eigenmode. Imperfect matching means that the field to be measured does not couple completely to the target optical resonance: the uncoupled fraction of light is reflected as if the resonator were a simple mirror, an effect that introduces an additional source of vacuum fluctuations in the quantum noise. It is not straightforward, however, to label such effect an "imperfection": in fact, it just makes the quantum operator slightly different, and may actually improve the access to two-mode features of the quantum state in some situations, as we have observed in our experiment. RD is able to surpass HD precisely because of vacuum modes added to certain spectral regions of the field; it is thus not surprising that adding vacuum modes in other ways could lead to beneficial results. For one thing, the spatial mismatch guarantees that there is always some light reaching the photodetector even at exact LO resonance ($\Delta = 0$), a feature that avoids the problem of technical noise at this detuning region. Finally, we note that a degenerate resonator (e.g., in confocal configuration) could effectively eliminate spatial mismatch effects on the quantum noise.

To model such situation, one must consider that the spatial mode of the impinging beam finds a decomposition with at least two contributing modes in the spatial basis privileged by the optical resonator. The positive part $\hat{E}^+$ of the input electric

field can be written as

$$\hat{E}^+(t) = \vec{F}_1(\vec{r})\,\hat{A}(t) + \vec{F}_2(\vec{r})\,\hat{B}(t), \tag{B1}$$

where $\hat{A}(t)$ is the target resonator spatial mode (i.e., the mode to which we aim to perfectly couple the impinging beam) and $\hat{B}(t)$ is a contamination mode. The vectorial functions $\vec{F}_j(\vec{r})$, $j = 1, 2, \dots$, stand for the spatial profile of the electric field in certain basis modes (e.g., Hermite-Gaussian spatial modes). The photocurrent operator $\hat{I}(t)$ is proportional to the integral of $\hat{E}^- \cdot \hat{E}^+$ on the surface of the photodetector, where the functions $\vec{F}_j(\vec{r})$ are assumed to respect orthonormality relations $\int \vec{F}_j(\vec{r}) \cdot \vec{F}_{j'}^*(\vec{r}) \mathrm{d}^2 r = \delta_{jj'}$, yielding

$$\hat{I}(t) = \hat{A}^\dagger(t)\hat{A}(t) + \hat{B}^\dagger(t)\hat{B}(t). \tag{B2}$$

In this spatial modal basis, the input quantum state of LO mode appears as $|LO\rangle = |\sqrt{1 - f^2}\,\alpha\rangle_1 |f\,\alpha\rangle_2$, where f^2 represents the fraction of modal contamination ($f = 0$ for perfect spatial mode matching). Performing the quantum state average of the observable of Eq. (B2) solely on the LO mode yields for the remaining spectral modes the photocurrent operator

$$\begin{aligned}
\hat{I}'(t) \approx{} & (1 - f^2)\,|\alpha|^2 + f^2 |\alpha|^2 \\
& + \sqrt{1 - f^2}(\alpha^* e^{i\omega_0 t}\,\hat{A}(t) + \alpha e^{-i\omega_0 t}\,\hat{A}^\dagger(t)) \\
& + f(\alpha^* e^{i\omega_0 t}\,\hat{B}(t) + \alpha e^{-i\omega_0 t}\,\hat{B}^\dagger(t)),
\end{aligned} \tag{B3}$$

where the prime superscript in $\hat{I}'(t)$ indicates that the quantum state average has already been performed on LO mode and only terms amplified by the LO have been kept. Disregarding the constant intensity contribution, the spectral photocurrent fluctuation is

$$\begin{aligned}
\hat{I}_\Omega ={} & \sqrt{1 - f^2}(\alpha^* \hat{A}_{\omega_0 + \Omega} + \alpha \hat{A}_{\omega_0 - \Omega}^\dagger) \\
& + f(\alpha^* \hat{B}_{\omega_0 + \Omega}(t) + \alpha\,\hat{B}_{\omega_0 - \Omega}^\dagger).
\end{aligned} \tag{B4}$$

Spatial mode mismatch implies that only the first term of Eq. (B4) undergoes the modal transformation of Eq. (A1) upon interaction with the resonator. The second term is assumed off-resonant (i.e., the resonance frequency ω_c is assumed to be mode dependent). The spectral operator transformed by Eq. (A1) and normalized by the LO amplitude reads as

$$\begin{aligned}
\hat{J}_\Omega(\Delta) ={} & \sqrt{1 - f^2}|r(\Delta)|(R_\Omega^*(\Delta)\hat{A}_\Omega + R_{-\Omega}(\Delta)\hat{A}_{-\Omega}^\dagger \\
& + \hat{J}_v) + f(\hat{B}_\Omega(t) + \hat{B}_{-\Omega}^\dagger),
\end{aligned} \tag{B5}$$

where the notation has been simplified in $\hat{A}_{\omega_0 \pm \Omega} \to \hat{A}_{\pm\Omega}$. To obtain the transformation of resonator detection as measured by the photodetection, it is necessary to change the spatial modal basis from $\{\hat{A}, \hat{B}\}$ back to the detection basis $\hat{a}$, according to

$$\hat{a}_\Omega = \sqrt{1 - f^2}\hat{A}_\Omega + f\hat{B}_\Omega, \tag{B6}$$

$$\hat{c}_\Omega = -f\hat{A}_\Omega + \sqrt{1 - f^2}\hat{B}_\Omega, \tag{B7}$$

where the basis $\hat{c}_\Omega$ of the spatial mode (assumed in the vacuum state) orthogonal to $\hat{a}_\Omega$ is necessary to perform the inverse modal transformation in Eq. (B5), yielding

$$\hat{J}_\Omega(\Delta) = G_\Omega^*(\Delta)\,\hat{a}_\Omega + G_{-\Omega}(\Delta)\,\hat{a}_{-\Omega}^\dagger + \hat{J}_v', \tag{B8}$$

where

$$G_\Omega(\Delta) = (1 - f^2)\,|r(\Delta)|\,R_\Omega(\Delta) + f^2 \tag{B9}$$

and the vacuum term is

$$\begin{aligned}
\hat{J}_v' ={} & f\sqrt{1 - f^2}[(1 - |r(\Delta)|\,R_\Omega^*)\hat{c}_\Omega + \\
& + (1 - |r(\Delta)|\,R_{-\Omega})\hat{c}_{-\Omega}^\dagger] + \sqrt{1 - f^2}|r(\Delta)|\hat{J}_v. \tag{B10}
\end{aligned}$$

[1] F. A. S. Barbosa, A. S. Coelho, K. N. Cassemiro, P. Nussenzveig, C. Fabre, M. Martinelli, and A. S. Villar, Phys. Rev. Lett. **111**, 200402 (2013).

[2] F. A. S. Barbosa, A. S. Coelho, K. N. Cassemiro, P. Nussenzveig, C. Fabre, A. S. Villar, and M. Martinelli, Phys. Rev. A **88**, 052113 (2013).

[3] R. E. Slusher, L. W. Hollberg, B. Yurke, J. C. Mertz, and J. F. Valley, Phys. Rev. Lett. **55**, 2409 (1985).

[4] L. A. Wu, H. J. Kimble, J. L. Hall, and H. F. Wu, Phys. Rev. Lett. **57**, 2520 (1986).

[5] A. Heidmann, R. J. Horowicz, S. Reynaud, E. Giacobino, C. Fabre, and G. Camy, Phys. Rev. Lett. **59**, 2555 (1987).

[6] B. L. Schumaker, S. H. Perlmutter, R. M. Shelby, and M. D. Levenson, Phys. Rev. Lett. **58**, 357 (1987).

[7] Z. Y. Ou, S. F. Pereira, H. J. Kimble, and K. C. Peng, Phys. Rev. Lett. **68**, 3663 (1992).

[8] A. S. Villar, L. S. Cruz, K. N. Cassemiro, M. Martinelli, and P. Nussenzveig, Phys. Rev. Lett. **95**, 243603 (2005).

[9] A. S. Coelho, F. A. S. Barbosa, K. N. Cassemiro, A. S. Villar, M. Martinelli, and P. Nussenzveig Science **326**, 823 (2009).

[10] Y. Shaked, Y. Michael, R. Z. Vered, L. Bello, M. Rosenbluh, and A. Pe'er, Nat. Commun. **9**, 609 (2018).

[11] Jiamin Li, Y. Liu, N. Huo, L. Cui, C. Feng, Z. Y. Ou, and X. Li, Opt. Express **27**, 30552 (2019).

[12] M. Manceau, G. Leuchs, F. Khalili, and M. Chekhova, Phys. Rev. Lett. **119**, 223604 (2017).

[13] X. Chen and Z. Y. Ou, Phys. Rev. A **102**, 032407 (2020).

[14] N. Takanashi, A. Inoue, T. Kashiwazaki, T. Kazama, K. Enbutsu, R. Kasahara, T. Umeki, and A. Furusawa, Opt. Express **28**, 34916 (2020).

[15] S. D. Bartlett, B. C. Sanders, S. L. Braunstein, and K. Nemoto, Phys. Rev. Lett. **88**, 097904 (2002).

[16] S. D. Bartlett and B. C. Sanders, Phys. Rev. A **65**, 042304 (2002).

[17] M. G. Genoni, M. L. Palma, T. Tufarelli, S. Olivares, M. S. Kim, and M. G. A. Paris, Phys. Rev. A **87**, 062104 (2013).

[18] E. H. Huntington, G. N. Milford, C. Robilliard, T. C. Ralph, O. Glockl, U. L. Andersen, S. Lorenz, and G. Leuchs, Phys. Rev. A **71**, 041802(R) (2005).

[19] A. S. Coelho, F. A. S. Barbosa, K. N. Cassemiro, M. Martinelli, A. S. Villar, and P. Nussenzveig, Phys. Rev. A **92**, 012110 (2015).

[20] T. C. Ralph, E. H. Huntington, and T. Symul, Phys. Rev. A **77**, 063817 (2008).

[21] G. Breitenbach, S. Schiller, and J. Mlynek, Nature (London) **387**, 471 (1997).

[22] J. Capmany and C. R. Fernández-Pousa, J. Opt. Soc. Am. B **27**, A119 (2010).

[23] D. T. Smithey, M. Beck, M. G. Raymer, and A. Faridani, Phys. Rev. Lett. **70**, 1244 (1993).

[24] A. I. Lvovsky and M. G. Raymer, Rev. Mod. Phys. **81**, 299 (2009).

[25] G. C. Bjorklund, M. D. Levenson, W. Lenth, and C. Ortiz, Appl. Phys. B **32**, 145 (1983).

[26] P. Galatola, L. A. Lugiato, M. G. Porreca, P. Tombesi, and G. Leuchs, Opt. Commun. **85**, 95 (1991).

[27] A. S. Villar, Am. J. Phys. **76**, 922 (2008).

[28] W. Schleich, *Quantum Optics in Phase Space* (Willey VCH Verlag, Berlin, 2001).

[29] E. Arthurs and J. L. Kelly, Jr., Bell Syst. Tech. J. **44**, 725 (1965).

[30] B. C. Young, F. C. Cruz, W. M. Itano, and J. C. Bergquist, Phys. Rev. Lett. **82**, 3799 (1999).

[31] R. W. P. Drever, J. L. Hall, F. V. Kowalsky, J. Hough, G. M. Ford, A. J. Munley, and H. Ward, Appl. Phys. B **31**, 97 (1983).